Distance measurements in Au nanoparticles functionalized with nitroxide radicals and Gd3+-DTPA chelate complexes

Author(s):
Yulikov, Maxim; Lueders, Petra; Warsi, Muhammad Farooq; Chechik, Victor; Jeschke, Gunnar

Publication date:
2012-08-14

Permanent link:
https://doi.org/10.3929/ethz-a-010784600

Originally published in:
Physical Chemistry Chemical Physics 14(30), https://doi.org/10.1039/c2cp40282c

Journal Name

Cite this: DOI:

ARTICLE TYPE

Distance measurements in Au nanoparticles functionalized with nitroxide radicals and Gd^{3+}-DTPA chelate complexes

Maxim Yulikov,[*a] Petra Lueders,[a] Muhammad Farooq Warsi,[b,c] Victor Chechik[*b] and Gunnar Jeschke[a]

Received (in XXX, XXX) Xth XXXXXXXXX 20XX, Accepted Xth XXXXXXXXX 20XX

DOI: 10.1039/b000000x

Nanosized gold particles were functionalised with two types of paramagnetic surface tags, one having a nitroxide radical and the other one carrying a DTPA complex loaded with Gd^{3+}. Selective measurements of nitroxide-nitroxide, Gd^{3+}-nitroxide and Gd^{3+}-Gd^{3+} distances were performed on this system and information on the distance distribution in the three types of spin pairs was obtained. A numerical analysis of the dipolar frequency distributions is presented for Gd^{3+} centres with moderate magnitudes of ZFS, in the range of detection frequencies and resonance fields where the high-field approximation is only roughly valid. The dipolar frequency analysis confirms the applicability of DEER for distance measurements in such complexes and gives an estimate for the magnitudes of possible systematic errors due to the non-ideality of the measurement of the dipole-dipole interaction.

Introduction

Nanometer range distance measurements based on the combination of site directed spin labelling (SDSL)[1] with pulse electron-electron double resonance[2], usually performed by a Double Electron-Electron Resonance (DEER) experiment[3] are nowadays broadly used to study structure and conformational changes of biomacromolecules.[4] The most common class of currently used spin labels are different modifications of nitroxide radicals. Due to the paramagnetism of many metal ions, their complexes also allow for EPR-based distance measurements, and a few studies on metalloproteins[5-7] and synthesized Cu^{2+}-containing compounds[8-11] were reported over the last decade.

The interest in Gd^{3+} chelate complexes as a possible alternative class of spin labels for pulse EPR distance measurements has been growing over the last few years because of a series of publications on high field DEER in pairs of Gd^{3+} centres.[12-17] Spin labelling with lanthanide chelate complexes has already been developed mainly for NMR purposes[18] and the main concepts could be transferred and adopted for the needs of pulse EPR techniques relatively easy and fast. Consequently only a short time was needed in the Gd^{3+}-Gd^{3+} DEER studies to step from model compounds[12,13] to labelled peptides/proteins[14-16] and nucleic acids.[17]

The Gd^{3+} centres have the particular feature of broadly distributed strengths and orientations of the zero field splitting (ZFS).[19,20] This leads to the absence of orientation selection effects in distance measurements and can be very valuable for high-field distance measurements.[14] Recently we reported the basic details about setup and performance of the DEER experiment in Gd^{3+}-nitroxide radical spin pairs.[21] We have demonstrated that this experiment can be performed down to X-band frequencies and that it is characterized by a much larger modulation depth as compared to DEER on Gd^{3+} pairs.

In its ground state[22], the Gd^{3+} ion has a spin 7/2. Therefore a formal description of the DEER experiment in this type of spin system has to deal with at least 8x8 density matrices (excluding couplings to magnetic nuclei and to the other electron spin). The effects arising due to the higher dimensionality of this spin system need to be analysed. In particular, due to multiple excited transitions, more than one value of the dipolar frequency should appear in the DEER experiment even for an ensemble of centres with exactly the same strength and orientation of ZFS's. Therefore if one considers the application of DEER for distance measurements with complexes that reveal relatively strong ZFSs as compared to the electron Zeeman (EZ) interaction, such that deviations from the high-field approximation become practically important, then the experimental data cannot be reliably analysed without numerical calculation of expected dipolar frequencies. Although some general theoretical consideration of the problem has already been reported[23], only qualitative discussion[12] and first order perturbation analysis[13] have been provided regarding high-spin Gd^{3+} centres. The mentioned discussion of the dipolar frequency distortions[12,13] refers to Kα- and W-band EPR measurements where usually no serious distortions of dipolar frequencies are expected, because the EZ term dominates over the ZFS term. For X-band measurements the ratio between ZFS and EZ scales up by a factor of 10 as compared to W band and a detailed analysis is required to verify the precision of DEER based distance measurements.

In this article we further develop methodology for using Gd^{3+} centers in combination with nitroxide radicals for distance measurements. In particular, a combination of selective distance measurements in nitroxide-nitroxide, Gd^{3+}-nitroxide and Gd^{3+}-

Gd^{3+} pairs is of potential interest for structural studies of macromolecules and other nanoobjects. Still, the application of these techniques to the intermediate frequency cases (X- and to some extent Q-band measurements) requires verification of the technique by numeric calculations of expected distance distortions.

This article has thus two main goals. First we aim to demonstrate experimentally and verify theoretically the possibility to measure distances by DEER on nitroxide-Gd^{3+} pairs using Gd^{3+} chelate complexes characterized by moderate ZFS to EZ ratios and therefore by rather broad EPR spectra. Second, we aim to demonstrate the potential of combining Gd^{3+} ions and nitroxide radicals to perform selective distance measurements in systems containing more than two spin centres. We show that Gd^{3+}-Gd^{3+}, Gd^{3+}-nitroxide and nitroxide-nitroxide distances can be measured independently from each other on the same sample. In this respect the present publication further develops the methodology for distance measurements in spectroscopically orthogonal spin pairs,[8,11,24] i.e. in pairs of non-identical paramagnetic centres, with each type of centres addressable selectively with some particular spectroscopic approach.

We used Au nanoparticles (AuNPs)[25] as a model system for distance measurements. A big advantage of these materials is the simple preparation and functionalization. Thus, particles containing a controlled average number of nitroxides and/or Gd^{3+} ions per AuNP can be readily prepared. The distributions of particle sizes and distances between paramagnetic tags on the AuNP surface are fairly broad; however, they can be quite accurately predicted from the electron microscopy images and analytical data. We have earlier showed the feasibility of nitroxide-nitroxide distance measurements in AuNPs by both cw[26] and pulse[27] EPR methods.

Experimental details

Synthesis and sample preparation

Au NPs can be readily prepared by the Brust *et al.* method[28] and functionalised using ligand exchange. Ligands **1** and **2** were thus used to introduce the nitroxide and chelating functionalities, respectively (Scheme 1). Synthesis of these ligands has been described previously.[25,29] We found, however, that hydrophilic AuNPs functionalised with the Gd^{3+} chelates **2** do not undergo ligand exchange with a hydrophobic ligand **1,** even if common solvents are used. The nitroxide group was therefore introduced by ligand exchange of ligand **1** with AuNPs coated with hydrophobic ligand **3** (which has *t*-Bu ester protecting groups). Acid deprotection of AuNPs was carried out under mild conditions in order to minimize degradation of the nitroxide functionality. Nevertheless, we found that *ca.* 50% of nitroxide was irreversibly destroyed during deprotection. The final nitroxide concentration was quantified by double integration of the cw EPR spectra at the end of synthesis and by measuring the depth of dipolar modulation in the nitroxide-nitroxide DEER experiment. The overall synthesis is shown in Scheme 1.

AuNPs stabilised by ligand **3** were synthesised by a modified Brust's biphasic method.[30] Tetraoctylammonium bromide (347 mg, 0.635 mmol) solution in toluene (12.0 mL) was added to the stirred 1.0 % (w/w) solution of hydrogen tetrachloroaurate trihydrate in water (5.0 mL, 0.127 mmol of Au). The mixture was stirred for *ca.* 5 min until all Au(III) precursor had transferred to the organic phase. A 10 % (w/w) solution of ligand **3** (107 mg, 0.127 mmol) in toluene was then added to the reaction mixture. A freshly prepared solution of $NaBH_4$ (48 mg, 1.27 mmol) in deionised H_2O (3.0 mL) was added 10 s after adding the ligand. Au(III) was reduced to Au(0) within seconds; the reaction mixture was stirred for further 10-15 min. The organic phase was separated from the aqueous phase and evaporated below 40°C to give a dark brown residue, which was dissolved in a minimum amount of toluene and purified by gel permeation chromatography using Bio-Beads SX-I gel (Bio-Rad) as a stationary phase and toluene as an eluent. Yield 75 mg.

The purified AuNPs were characterized by UV/Vis. spectroscopy (surface plasmon band was observed at 520-525 nm), transmission electron microscopy (TEM) (average diameter 2.42 nm, width of AuNP size distribution ±0.34 nm, see supplementary information) and thermogravimetric analysis (TGA) (47% organic contents). From TGA and TEM data, the average composition of the gold nanoparticles protected by ligand **3** was estimated as $Au_{439}Ligand_{88}$.

The spin labelling of AuNPs was done by ligand exchange using a modified literature procedure.[31] AuNPs coated with ligand **3** (50.0 mg, 0.027 mmol of diethylene triamine pentaacetic acid (DTPA) units) were dissolved in dimethylformamide (10.0 mL). To the stirred solution of AuNPs, a 1.0 mM solution of ligand **1** (0.8 mL, 7.85×10^{-4} mmol) was added. The reaction mixture was stirred overnight at 60°C. The solvent was evaporated using a rotary evaporator, and the spin labelled AuNPs were purified by gel permeation chromatography using Bio-Beads SX-I gel (Bio-Rad) as a stationary phase and dichloromethane (DCM) as an eluent. Yield 35 mg.

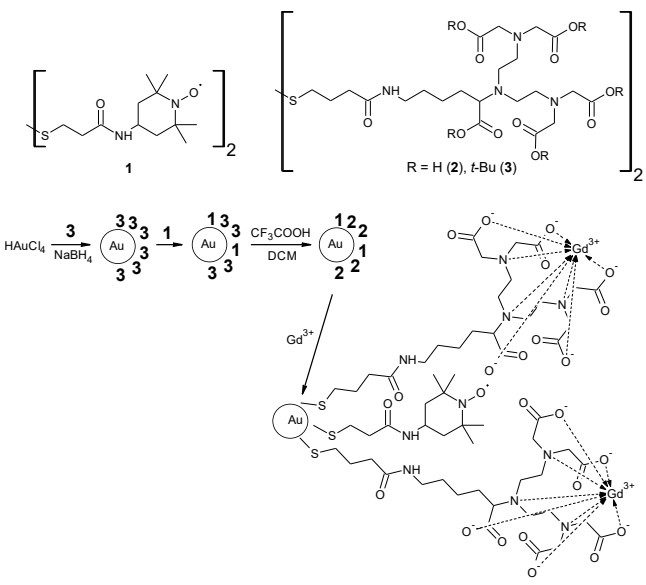

Scheme 1 Synthesis of AuNPs tagged with paramagnetic groups

Deprotection of *t*-Bu ester groups was carried out using a modified literature procedure.[32] Trifluoroacetic acid (4.0 mL) was syringed into a solution of spin labelled AuNPs (35.0 mg) in DCM (8.0 mL) under inert atmosphere. After stirring for 3-4 h, solvent was evaporated at room temperature using a rotary

evaporator and the residual acid was immediately quenched with 0.1 M NaOH. Deprotected spin labelled AuNPs were dialysed against deionised water overnight and then purified by gel permeation chromatography using Sephadex gel (G 100) as a stationary phase and deionised water as an eluent. Yield 23.0 mg.

Complexation of Gd^{3+} with DTPA units of the ligand attached to AuNPs was carried out by a modified literature procedure.[33] A 1.0 mM aqueous gadolinium chloride hexahydrate solution was added dropwise to a 10.0 mL aqueous AuNPs coated with a mixture of ligands **1** and **2** (15.0 mg) over a period of 10 min. The amount of free Gd^{3+} was monitored by colorimetric titration with xylenol orange. The reaction mixture was then stirred for further 30 min. The pH of the medium was kept slightly basic (8-9) during addition of Gd^{3+} using aq NaOH. After addition of Gd^{3+}, water was evaporated below 40°C to get a dark brown powder. The free Gd^{3+} ions were removed by dialyzing the aqueous solution of Gd^{3+}-loaded AuNPs against deionised water. The water was then evaporated below 40°C using rotary evaporator to get solid Gd^{3+}-loaded AuNPs. Yield 11.23 mg.

Table 1. List of studied samples and estimates of labelling efficiencies for nitroxide radicals and Gd^{3+} ions.

Sample	Average # of active nitroxides per AuNP: From CW EPR	From NO-NO DEER modulation depth	From Gd^{3+}-NO DEER modulation depth	# of Gd^{3+} centers per AuNP
32% La	0.2-0.4	0.46	—	—
0% Gd	0.2-0.4	0.24	—	—
2% Gd	0.2-0.4	0.46	0.36	1.6
4% Gd	0.2-0.4	0.3	0.3	3.2

In the final composition, AuNPs contained on average 80 DTPA-based ligands and 0.2-0.4 active nitroxides. AuNPs were loaded with 0%, 2% and 4% of Gd^{3+} with respect to the total number of DTPA-based ligands, which corresponds approximately to the average compositions of 0, 1.6 and 3.2 Gd^{3+} ions per particle. An additional sample with AuNPs loaded with 32% of diamagnetic La^{3+} was used for supplementary measurements. For pulse EPR measurements dispersions of about 100 μM of AuNPs in 1/1 v/v mixture of H_2O and glycerol were prepared and shock-frozen in liquid nitrogen. The EPR samples of approximately 50 μl volume in 3 mm outer diameter quartz tubes were then stored at 77 K. The sample types and approximate numbers on nitroxide radicals and Gd^{3+} centers per AuNP are listed in Table 1.

EPR measurements and their processing

The X-band pulse EPR measurements were performed with Bruker Elexsys II E680 X/Q-band spectrometer with an ER 4118X - MS3 resonator (split ring resonator, mw frequency 9.6 GHz, maximum allowed diameter of a cylindrical sample 3 mm). The Q band measurements were performed at a home-built Q-band spectrometer[34] with a rectangular cavity which allows for oversized samples.[35] Gd^{3+}-nitroxide and Gd^{3+}-Gd^{3+} DEER measurements were performed at 10 K whereas the nitroxide-nitroxide DEER was performed at 50 K. In both cases the measurement temperature corresponded approximately to the optimum measurement conditions with respect to the longitudinal and transverse relaxation of Gd^{3+} ions (10 K) or nitroxide radicals (50 K). Sample temperature was stabilized with a He-flow cryostat (ER 4118 CF, Oxford Instruments).

The maximum load of Gd^{3+} was limited to 4%, which corresponded roughly to an average of about 3.2 Gd^{3+} ions per AuNP in order to avoid strong multispin contributions. The Gd^{3+}-Gd^{3+} DEER was measured only on the sample with 4% loading, i.e. approximately 3.2 Gd^{3+} ions per AuNP. The modulation depth in this experiment was about 0.04. Reducing the loading would result in yet lower modulation depth and would make the extraction of the form factor problematic.

The pulse settings for the nitroxide-nitroxide and Gd^{3+}-nitroxide DEER experiment reproduce the optimum settings used in our previous work.[21] The settings for the Gd^{3+}-Gd^{3+} DEER were analogous to the ones used in original works[12] with the modification of having the detection frequency on the other (high-field) side of the central peak of the Gd^{3+} EPR spectrum in order to avoid its overlap with the EPR spectrum of nitroxide radicals. Use of such a set-up has also been proposed in addition to the original one in order to increase the modulation depth obtained in the Gd^{3+}-Gd^{3+} DEER.[17] All pulses were set to a duration of 12 ns except of nitroxide-nitroxide DEER at X band where pump pulse of 12 ns and all detection pulses of 32 ns were used. The first interpulse delay time in the DEER sequence was set to 400 ns in all cases. The second delay time (between the primary echo and refocusing pulse) was set according to the required length of DEER trace, which was selected to provide sufficient range for background correction. Typical measurement time was 15-25 hours for X-band measurements and 3-6 hours for Q-band measurements, depending on the required signal-to-noise ratio.

For nitroxide-nitroxide DEER the offset between pump and detection frequencies was +65 MHz at X band and -85 MHz at Q band. For Gd^{3+}-nitroxide DEER the offset between pump and detection frequencies was -80 MHz at X band and -300 MHz at Q band. For Gd^{3+}-Gd^{3+} DEER, measured only at Q band, the offset between pump and detection frequencies was -200 MHz.

Figure 1A shows the positions of the pump and detection frequencies used at Q band for separate detection of the distance distributions in the three types of spin pairs.

Echo detected (ED) EPR spectra of Gd^{3+} ions measured at X and Q band were compared to simulations for a series of EPR spectra computed for different fixed *D*-values of the ZFS interaction with *E*-values distributed according to the probability function $P(E/D)=(E/D)-2\cdot(E/D)^2$ (for the origin of this probability distribution see the description given in the numeric analysis section). The comparison shown in Figure 1B suggests characteristic *D*-value of about 1500 MHz for the Gd^{3+}-complex studied.

Fitting of DEER data was performed with DeerAnalysis 2009 software.[36] In order to avoid possible artefacts, the range for the background fit was set to end at least 100 ns before the end of the DEER trace. At X band the optimum value of the background dimension for the fits presented in the paper was always in the range from 3.0 to 3.1 for all samples. The results of fitting were not sensitive to a change of the background dimension in a broader range (2.9-3.2). At Q band longer DEER traces could be obtained and the optimum background dimension was ranging

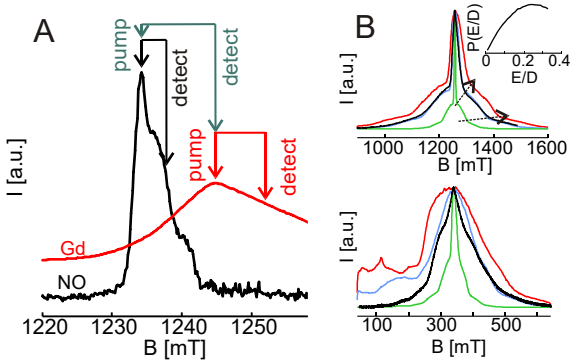

Figure 1 (A) Q-band ED EPR spectra of Gd3+ ions (red) and nitroxide radicals (black). Pulse positions for the DEER experiments at Q-band frequencies are marked with red arrows for the Gd3+-Gd3+, green arrows for the Gd3+-nitroxide, and black arrows for the nitroxide-nitroxide DEER. (B) Fit of ED EPR spectra of Gd3+ ions at Q-band (top) and X-band (bottom). Experimental spectrum is shown in black. Simulations are shown for Gaussian distributions of D with <D>=600 MHz (green), 1500 MHz (blue) and 2000 MHz (red). The width σ(D) was set to be <D>/10 in all simulations. The distribution of E/D is shown in the inset of the upper plot.

between 3 and 6.2 for different experiments. Still the actual differences in background functions were not dramatic due to relatively slow background decay and rather clear separation between the form factor and the background. The obtained distance distributions were stable with respect to the change of the background function within the mentioned range of background dimensions.

All traces were fitted both with sphere surface model, which is incorporated into DeerAnalysis 2009, as well as with unrestricted distance distribution. In the latter case Tikhonov regularization[37-39] has been performed and distributions corresponding to different regularization parameters were analysed.

Calculations

The dipolar frequency calculations were performed with MATLAB software using a home-written program. The spin Hamiltonians were built and diagonalized with help of corresponding functions from the EasySpin package.[40] Distributions of dipolar frequencies were calculated for the high temperature limit, which is a good approximation at 10K for both X- and Q-band EPR experiments: at 10K the thermal energy kT is still significantly larger than the Zeeman energies in the corresponding magnetic fields. Multidimensional integrations (over two polar angles and two parameters of the ZFS term) were performed with a Monte-Carlo type algorithm, where all integration variables were randomly changing on each step. Summation over at least 50,000 steps has been done and the results were proven to be stable upon further increase of the number of Monte-Carlo steps.

In order to visualize the distortions arising due to the ZFS interaction, DEER traces were generated out of the distorted dipolar frequency patterns for different combinations of D and E values. For that a fixed single distance of 3.0 nm was assumed, and the dipolar frequency patterns were scaled accordingly.

Excitation bandwidth correction was always performed assuming excitation frequency of 9.474 GHz and a Gaussian excitation profile with the width of 100 MHz. All resonance frequencies were computed in the magnetic field of 340 mT.

The ED EPR spectra of Gd^{3+} ions with distributed D- and E-parameters of the ZFS interaction were calculated based on EasySpin package for a finite temperature of 10 K.

Numerical analysis of the data

Analysis of dipolar frequencies: theoretical background

In order to verify the applicability of the DTPA-based Gd^{3+} complexes for reliable distance measurements with the DEER experiment at X- and Q-band frequencies, we performed a series of calculations and determined the level of dipolar frequency distortions for complexes with different strengths of ZFS interaction. Such analysis is required since typical zero-field splittings in Gd^{3+} complexes with macrocyclic ligands lead to substantial level mixing, in particular at X-band. With such strong mixing, our previous finding of a rather precise distance measurement at X band[21] may appear fortuitous and cannot be generalized without theoretical analysis.

In analysis we restrict ourselves to situations where the characteristic frequencies of magnetic dipole-dipole interaction between two spins are sufficiently small compared to the frequency offset between the pumped and the detected species. This is a typical assumption for the analysis of DEER data and for the frequency offsets used at X band (80-85 MHz) and Q band (300 MHz) it should hold for a major fraction of spins. The situation may change for very short distances, where dipolar frequencies become comparable to the frequency offset. A discussion of possible consequences of this has been given on an example of Gd^{3+}-Gd^{3+} DEER.[13] If the above assumption holds true, then the effect of the dipole-dipole interaction on the resonance frequencies of EPR transitions can be computed from the secular part of the dipolar term in spin Hamiltonian.

The eigenstates of the spin system can then be computed from a zero-order Hamiltonian consisting of the EZ term $\mathbf{H}_{EZ}$ and the ZFS term $\mathbf{H}_{ZFS}$. The weaker hyperfine and nuclear Zeeman interactions can be dropped out in this computation. In the high-field approximation, the ZFS term has been treated by perturbation theory.[41] This approach is sufficient for discussing high frequency EPR measurements, performed at electron transition frequencies of about 95 GHz (W band) or higher. In most cases this approach also works for Q/Kα bands, corresponding to the electron resonance frequencies in the range of 30-36 GHz. At the currently still most common EPR frequencies of 9-10 GHz (X band) the relative amplitudes of the EZ and ZFS terms are often of the same order of magnitude, with the ZFS term still being a few times weaker than the EZ term. In the present discussion we are interested in analysing this limiting situation and thus no assumptions were made on relative strength of EZ and ZFS interactions. Instead an exact solution of the eigenstates problem has been computed numerically for each orientation of the ZFS tensor with respect to the external magnetic field and for each set of characteristic values, defining the strength of the ZFS-term.

For a Gd^{3+} ion with spin 7/2 terms including 2nd, 4th and 6th power of spin operators can appear in the ZFS-part of the spin Hamiltonian. Still, from the cases where all these terms were experimentally determined[42] it is apparent that 4th and 6th order terms are sufficiently weak and would not be able to break the high-field approximation. Additionally, in glassy frozen solution a distribution of the second order ZFS parameters is always observed,[19,20] which reflects the pattern of dynamic rearrangements of the chelator molecules around the Gd^{3+}-ions in the solution before freezing. Therefore it is usually difficult to experimentally determine the higher order terms of the ZFS interaction for glassy samples and a description with a distribution of second order ZFS parameters appears to be the most appropriate. For a single set of the second order ZFS parameters D and E the corresponding term in the spin Hamiltonian can be written in its eigensystem as

$$\mathbf{H}_{ZFS} = D\left[\mathbf{S}_Z^2 - \frac{1}{3}S(S+1)\right] + E\left[\mathbf{S}_X^2 - \mathbf{S}_Y^2\right]. \qquad (1)$$

For an arbitrary orientation of the ZFS tensor with respect to the external magnetic field all three spin operators S_X, S_Y and S_Z have non-zero projections on each eigenstate of the zero-order spin Hamiltonian, which modifies the secular contribution of the dipole-dipole interaction as compared to a pair of spin 1/2 species.

The general equation of the dipole-dipole term in the spin Hamiltonian is given by[43-45]

$$\mathbf{H}_{dd} = \frac{\mu_0}{4\pi\hbar r^3}\left[(\vec{\mu}_1,\vec{\mu}_2) - \frac{3}{r^2}(\vec{\mu}_1,\vec{r})(\vec{\mu}_2,\vec{r})\right]. \qquad (2)$$

The relation between the magnetic moment operator and the dimensionless spin operator for each species is

$$\vec{\mu}_{1,2} = g_{1,2}\mu_B\hbar\vec{\mathbf{S}}_{1,2}. \qquad (3)$$

Here vector operators $\hat{\vec{\mu}}_{1,2}$ describe point magnetic dipoles attributed to the two paramagnetic centres and $\vec{r}$ is the interspin vector. For a pair S_1=1/2, S_2=1/2 (for instance, two nitroxide radicals) the high field approximation is usually valid and the EZ term dominates the spin Hamiltonian. In this case, if we set the direction of external magnetic field along the z-axis and neglect the anisotropy of the g-tensor, which is also a fairly good approximation for nitroxide radicals, the secular part of Eq. (2) is given by[45]

$$\mathbf{H}_{dd}(sec.) = \frac{\mu_0\hbar g_1 g_2\mu_B^2}{4\pi r^3}\mathbf{S}_{Z,1}\mathbf{S}_{Z,2}\left[1-3\cos^2\theta\right] = \omega_{dd}\mathbf{S}_{Z,1}\mathbf{S}_{Z,2}\left[1-3\cos^2\theta\right] \qquad (4)$$

In the DEER experiment this secular term determines the observed dipolar frequency for a pair of spin 1/2 species for most of the situations except for the case mentioned above, where the resonance frequencies of the two spins are close to each other, such that non-secular terms in the dipolar interaction become comparable to the resonance frequency difference. The spin echo detected in the experiment is modulated with the difference of the two single quantum transition frequencies of the observer spin (S_1) with the pump spin (S_2) being in either the S_Z=+1/2 or in the S_Z=-1/2 state. For instance for θ=0, the two dipolar corrections to the resonance frequency are $\pm\omega_{dd}/2$ and the DEER echo is modulated with the frequency difference, which is equal to ω_{dd}.

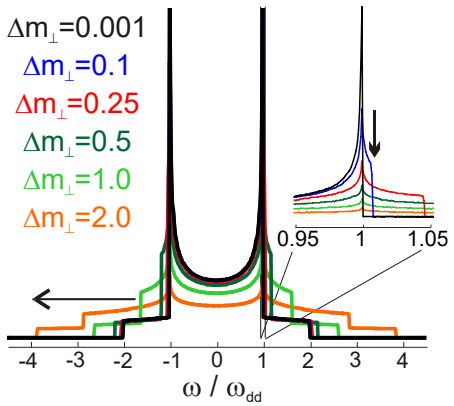

Figure 2 Distorted Pake-like dipolar frequency distributions computed from the Eq. (7) with Δm||=1.0 and with different Δm⊥ as indicated on the figure.

For an arbitrary orientation of the spin-spin vector with respect to the external magnetic field, the two dipolar frequencies are given as

$$\omega_{1,2}(\theta) = \pm\frac{\omega_{dd}}{2}\left[1-3\cos^2\theta\right] \qquad (5)$$

These undisturbed equations for the two frequencies when summed together and averaged over all orientations of the interspin vector form the "classical" Pake pattern[43-46]. This type of function is implemented in the DeerAnalysis software[36] and since that program or an equivalent approach is commonly used to analyze the experimental data, we need to compute the deviations of the dipolar frequency patterns in the Gd^{3+}-nitroxide spin pairs from the unperturbed Pake pattern, generated using Eq. (5).

For computing the dipolar frequencies observed in Gd^{3+}-nitroxide DEER measurements one has to perform two step calculations for each EPR transition of the Gd^{3+} centre. In the first step, the frequency of a given transition of the Gd^{3+} centre has to be computed for the cases of spin-up and spin-down state of the nitroxide radical. The dipolar modulation frequency observed in the DEER experiment is then computed as a difference $\Delta\omega$ of these two transition frequencies. Modulation with frequencies $\pm\Delta\omega$ occurs corresponding to the situations where the nitroxide spin is flipped from $|\alpha\rangle$ to $|\beta\rangle$ state or *vice versa*. In the second step, the distorted dipolar frequency pattern is obtained as a histogram of $\pm\Delta\omega$ for all orientations of the interspin vector. Mathematically the problem can again be reduced to calculations of the differences of diagonal matrix elements for the spin operators of Gd^{3+}-centres (S_1-spin, detection) and of nitroxide radicals (S_2-spin, pump). In the Gd^{3+}-nitroxide spin pair one can still assume that the high-field approximation is strictly valid for the nitroxide species. Therefore, only terms proportional to the $S_{Z,2}$ operator need to be considered in the secular part of the dipolar interaction, and the projections of this operator for the two eigenstates of the nitroxide spin can be assumed to be exactly ±1/2. For Gd^{3+} centres we keep the ZFS term in the spin Hamiltonian, assuming no particular relation between the strength of this term and of the

EZ interaction term. In this case all three projections of the Gd^{3+} spin operator would contribute to the secular part of the dipolar interaction. This leads to the equations

$$\mathbf{H}_{dd}(sec.) = \omega_{dd}\left[(\mathbf{S}_{Z,1})_{sec.}\,\mathbf{S}_{Z,2} - \frac{3}{r}\left(\vec{\mathbf{S}}_1,\vec{r}\right)_{sec.}\mathbf{S}_{Z,2}\cos\theta\right] \quad (6)$$

$$\omega_{1,2}(\theta) = \pm\frac{\omega_{dd}}{2}\left[\Delta m_Z\left(1-3\cos^2\theta\right) - 3\Delta m_X\cos\theta\sin\theta\cos\phi - 3\Delta m_Y\cos\theta\sin\theta\sin\phi\right]. \quad (7)$$

The values Δm_X, Δm_Y and Δm_Z refer to each particular transition of Gd^{3+} and can be computed as differences of the diagonal elements of operators S_X, S_Y and S_Z after transformation to the eigenframe of $\mathbf{H}_{EZ}$ + $\mathbf{H}_{ZFS}$. For example, if transition between eigenstates |i⟩ and |j⟩ is considered, then $\Delta m_X = \langle j|S_X|j\rangle - \langle i|S_X|i\rangle$ *etc*. For each particular orientation of the eigenframe of the Gd^{3+} centre a dipolar frequency pattern is formed by summing up all possible orientations of the spin-spin vector with respect to the principal axes of this frame. Without loss of generality one can in each case redefine the coordinate system (x', y', z') for the spin Hamiltonian such that Δm_y becomes zero and the perpendicular component of the magnetization difference is directed along the x'-axis of the new coordinate frame. The polar angle φ describing the orientation of the interspin vector would get a constant phase shift by such transformation. This shift is not important due to the summation over all orientations of the spin-spin vector. Therefore the dipolar frequency pattern in the Gd^{3+}-nitroxide spin pair can be characterized by two parameters $\Delta m_{\|} = \Delta m_Z$ and $\Delta m_{\perp} = (\Delta m_X^2 + \Delta m_Y^2)^{1/2}$ in the following manner:

$$\omega_{1,2}(\theta) = \pm\frac{\omega_{dd}}{2}\left[\Delta m_{\|}\left(1-3\cos^2\theta\right) - 3\Delta m_{\perp}\cos\theta\sin\theta\cos\phi\right]. \quad (8)$$

In the absence of level mixing $\Delta m_{\|}$=1.0 and $\Delta m_{\perp}$=0. The interplay between ZFS and EZ terms in spin Hamiltonian breaks these relations and distorts the dipolar frequency pattern. The deviations of $\Delta m_{\|}$ from 1 lead to a shift of the apparent distance from the real one in the distance analysis. The dipolar frequency pattern in this case stretches proportionally to the actual value of $\Delta m_{\|}$ and does not change its shape. On the other hand, the non-zero values of $\Delta m_{\perp}$ result in deviations of the shape of the dipolar frequency pattern from the unperturbed Pake case. Figure 2 shows a few examples of such patterns computed for $\Delta m_{\|}$=1 and for several relevant values of $\Delta m_{\perp}$.

Analysis of dipolar frequencies: numeric simulations

The numerical computations were performed for X-band frequencies (9.474 GHz), but the problem essentially depends only on the ratio $3D/g\mu_B B$. Therefore the presented figures can be used for other bands after scaling up the corresponding D-values according to the increase of the measurement frequency. We used the value $3D/g\mu_B B$ as a measure of the quality of the high field approximation, because this value appears as a pre-factor in the first order perturbation equations for the expectation values of perpendicular projections of the Gd^{3+} spin operator[41] and thus determines the magnitude of the distortion of the dipolar frequency pattern.

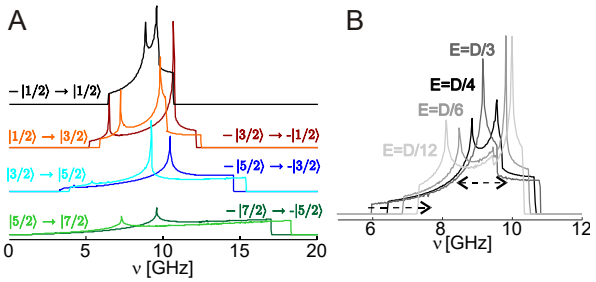

Figure 3 (A) Transition separated distributions of resonance frequencies simulated for Gd3+ ions with D=1500 MHz and E=D/4 (375 MHz). (B) Simulated resonance frequency distributions for the |-1/2>↔|+1/2> transition of Gd3+ ions with D=1500 MHz and E values as indicated on the plot.

Figure 3 shows distributions of the resonance frequencies computed separately for each single quantum transition of a Gd^{3+} centre with D=1500 MHz. Experimentally in the DEER pulse sequence only a fraction of species with resonance frequencies close to the centre of the |-1/2>↔|+1/2> transition is excited. Accordingly the contribution of each transition to the DEER signal reduces with the increase of the width of its frequency distribution.

The width of the central (|-1/2>↔|+1/2>) transition of Gd^{3+} complexes with weak ZFS and E~0 can be approximately computed as $f{\cdot}D^2/g\beta B$[47,48], with a numeric factor f in the range between 10 and 13. For larger E-values the apparent width of this transition is yet somewhat reduced because of lower intensities at the left and right shoulders and because of the shift of the maxima towards the centre of the transition pattern (Figure 3B). For Gd^{3+} centres with small ratios of the ZFS *vs*. EZ term, this transition forms a pronounced sharp peak in the centre of the EPR spectrum. If detection is performed at the maximum of this peak, then the central transition has the biggest contribution to the obtained signal. The first order perturbation theory treatment performed for half integer high-spin centres[20,41] predicts zero differences in the projections of $\mathbf{S}_X$ and $\mathbf{S}_Y$ operators between the eigenstates with S_Z=±1/2. Still, even for these cases the contribution of transitions other than |-1/2>↔|+1/2> is not negligible and possible distortions of the distance distribution need to be analysed.

For cases where the difference between ZFS and EZ contributions is less than an order of magnitude, the relative contribution of transitions that include eigenstates with absolute values of S_z higher than 1/2 grows because of the broadening of the central peak. At the same time, because of the weakening of the high-field approximation the first order perturbation treatment gets insufficient and an analysis based on exact calculations (or at least up to higher orders of the perturbation theory) is required. In practice the EPR spectra of typical chelate complexes of Gd^{3+}, detected at Q band (34-35 GHz) and at yet higher frequencies do show a pronounced central peak. This central peak is usually not distinguishable if the measurements are performed at X band (9-10 GHz). This indicates that the relative ratio between ZFS and EZ terms in this case lies in a a problematic range.

In particular formation of the Gd^{3+}-DTPA complex requires 1-2 extra water molecules to fill all coordination positions around the Gd^{3+} ion. Thus the local symmetry strongly deviates from the cubic one, which leads to rather large values of D for DTPA

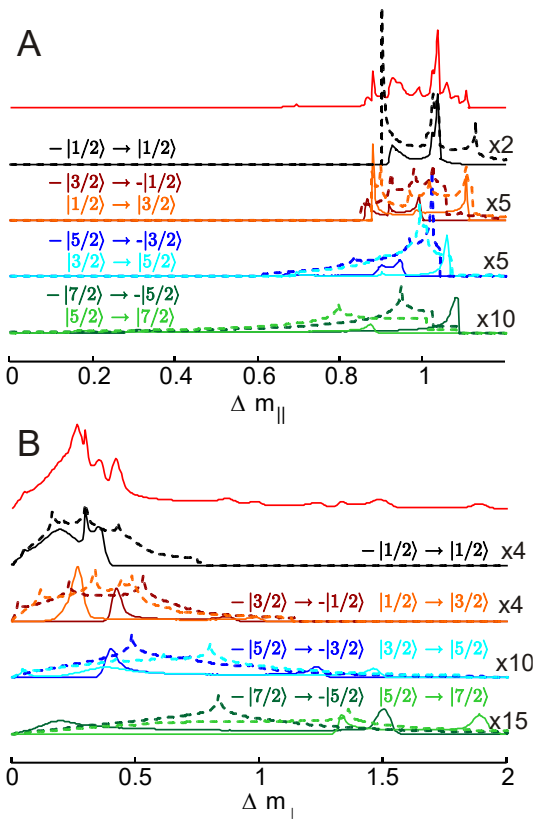

Figure 4 Transition separated distributions of Δm|| (A) and Δm⊥ (B) simulated for Gd3+ ions with D=1500 MHz and E=D/4 (375 MHz). Dotted lines indicate full distributions. Solid lines show the distributions corrected for a Gaussian excitation profile with a width of 100 MHz. The upper red curves show the sums of the excitation corrected distributions over all 7 transitions.

complexes.[19,49] As one of the examples in our dipolar frequency analysis we have chosen the value of D=1500 MHz ($3D/g\mu_B B \approx 0.5$ at X band), which leads to the EPR spectrum of a width comparable to our experimentally detected spectra of Gd^{3+}-DTPA complexes (Figure 1B) and agrees with the literature data for this ligand[19,49]. Thus this particular D-value is relevant for the presented Gd^{3+}-nitroxide DEER data measured with DTPA-based Gd^{3+} complexes. Further examples, covering the range of D values from $3D/g\mu_B B \approx 0.7$ down to $3D/g\mu_B B \approx 0.1$ are given in the Supplementary Material. Below the ratio of 0.1 first order perturbation analysis seems to be sufficiently precise and the corresponding dipolar frequencies can be computed in a compact analytical form.[13] Besides, as it will be apparent from the following discussion, for these cases the deviations in the DEER experiment are expected to be negligibly small.

A single value of E/D is not capable to describe the experimentally observed bell-like shape of the Gd^{3+} EPR spectrum.[19,20] We assumed for each value of D a distribution of E values according to a probability function[19,20] $P(E/D)=(E/D)\cdot 2\cdot(E/D)^2$. This distribution was obtained from the Monte-Carlo simulations of Gd^{3+} complexes with completely free mutual arrangement of chelating moieties and may not be exactly valid for the DTPA case, where different chelating moieties are connected to each other via chemical bonds. Still this distribution reflects key features of the system. The fraction of complexes with nearly axial symmetry ($E\approx 0$) should be rather small, as it implies a special arrangement of ligands. As the glassy sample reflects a pattern of dynamic rearrangements of complexes in solution, it should contain mainly distorted ligand configurations with lowest (tetragonal) symmetries. Experimentally this leads to a single peak pattern for the central transition. In case of dominating species with $E\approx 0$, a double peak pattern would have been expected. The main results of the following analysis are not sensitive to small changes of the shape of the E/D-distribution as long as the values of E/D~1/3-1/4 are the most probable and the ones with E/D~0 are suppressed.

It the first step of analysis we shall discuss the dependence of $\Delta m_\perp$ and $\Delta m_\parallel$ distributions on the E-value for a fixed D. An example calculated for D=1500 MHz and $E=D/4$ is given in Figures 4. Further calculations are presented in the Supplementary Material. Calculations for different values of D lead to qualitatively analogous pictures with the widths of $\Delta m_\perp$ and $\Delta m_\parallel$ distributions scaling accordingly. Figures 4A and 4B represent the distributions of $\Delta m_\perp$ and $\Delta m_\parallel$ constructed for each of the seven transitions of Gd^{3+}. If a correction for finite excitation bandwidths of the microwave pulses is taken into account, the distributions get narrower. The effect of the excitation bandwidth on the widths of $\Delta m_\perp$ and $\Delta m_\parallel$ distributions is not very strong, because in most cases the angular dependence of the resonance frequency for a given transition does not fit to the ones for $\Delta m_\perp$ and $\Delta m_\parallel$. The shape of the EPR signal of the central transition for the complexes with E/D~0 has a minimum at around the g-value position for Gd^{3+}-centres, where detection is performed. Because of this particular feature the relative contribution of the central transition for those species is reduced and thus the deviations of $\Delta m_\perp$ and $\Delta m_\parallel$ from the ideal values of 0 and 1 are higher than for the cases of larger ratios E/D. If such complexes appear to dominate in experiment, the situation may be improved by shifting the detection position to a more advantageous frequency/field.

Qualitatively, the extreme values of $\Delta m_\perp$ and $\Delta m_\parallel$ and the widths of their distributions increase when increasing the absolute values of S_z of the two eigenstates corresponding to the transition under consideration. For the value of $3D/g\mu_B B\approx 0.5$ ($D\approx$1500 MHz at X band), the central transition still provides the biggest fraction of the detected signal, but the contributions from the two $|\pm 1/2\rangle \leftrightarrow |\pm 3/2\rangle$ transitions are comparably big and even the outermost transitions $|\pm 5/2\rangle \leftrightarrow |\pm 7/2\rangle$ contribute considerably (Figure 4).

A detailed set of illustrations for each separate transition for the case of fixed D and distributed E-values is given in the Supplementary Material for D=1100, 600 and 300 MHz. The calculations reproduce the qualitative picture discussed for the situation with fixed D and E values. The corresponding full absorption spectra and the distributions for $\Delta m_\perp$ and $m_\parallel$, summed over all seven transitions are given as well.

One would expect that stronger ZFS would induce stronger level mixing and thus larger deviations from the non-disturbed case. The numeric calculations confirm that the worst case is represented by the largest ZFS parameter D=2000 MHz ($3D/g\mu_B B\approx 2/3$). It is important to notice that already for the case $3D/g\mu_B B\approx 1/3$ (D=1100 MHz) the distortions of $\Delta m_\parallel$ are rather modest and for the majority of orientations and E/D ratios they

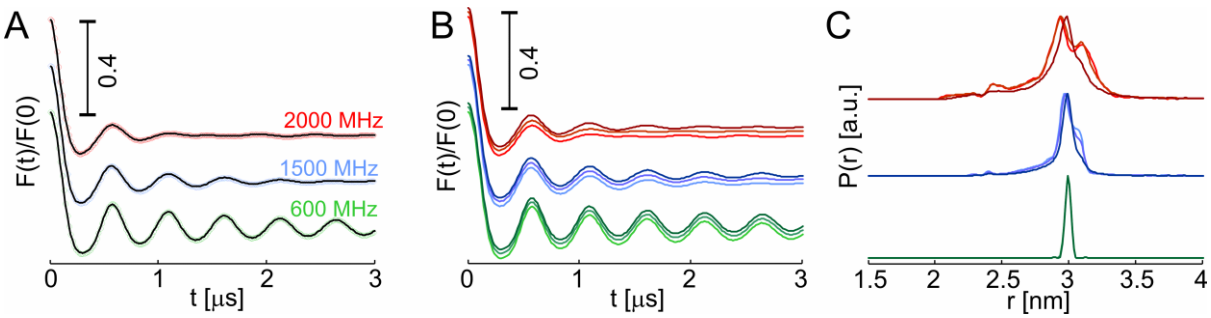

Figure 5 DEER traces and distance distributions resulting from the ZFS-distorted dipolar frequency patterns. All dipolar frequency patterns were constructed, assuming a single distance equal to 3.0 nm. (A) DEER traces constructed out of distorted dipolar frequency patterns for fixed D=600 MHz (green), 1500 MHz (blue) and 2000 MHz (red). E/D was distributed according to the description in the text of the article. Best fits of the three DEER traces with DeerAnalysis are shown in black. The DEER traces are vertically shifted for better visualisation. (B) Comparison of DEER traces for the three mean values of D as in (A) and for the width of gaussian distribution for D values equal to zero (lower trace, light color), D/10 (middle trace, intermediate color) and D/4 (upper trace, dark color). (C) Distorted distance distributions obtained from the DEER traces from (B) with use of DeerAnalysis software. The same color code as in (B) is used.

are within the 10% range around the non-distorted value of 1.0. Because of the conversion of the dipolar frequency to the distance via a cube-root relation (see Eq. (4)), the corresponding distortions of the distance would be within approximately 3% from the actual value. This would lead to an artificially broadened distance distribution of a width of about 0.15 nm for a distance of 5 nm and of about 0.3 nm for a distance of 10 nm. For the majority of cases, and especially for distance measurements in biomacromolecules, this distortion would not be experimentally detectable due to significantly bigger widths of the obtained distance distributions. For lower values of D one can safely neglect the distribution of $\Delta m_{\|}$ values for any type of distance measurements even with completely rigid arrangements of spin labels.

For D≈1500 MHz and distances up to 4-5 nm as in our study the deviation of $\Delta m_{\|}$ from 1.0 reaches up to 20% (the value of $\Delta m_{\|}$ ranges between 0.8 and 1.2 and even beyond that, Figure 4A), which means a distortion of obtained distances up to 6% or 0.3 nm at a distance of 5 nm. The average deviation of $\Delta m_{\|}$ is even less in this case, therefore the experimental precision of distance measurements should be yet better.

The distribution of $\Delta m_{\perp}$ values for D=1500 MHz appears to be significantly more distorted and reveals a significant fraction of species with $\Delta m_{\perp}$ values more than 1.0. Still, a sufficient fraction of the orientations falls into the range $\Delta m_{\perp}$~0.1-0.5, which one can assume to be moderately small. The actual distortion of the distance measurement was analysed by constructing a Pake-like dipolar frequency pattern from this distribution of $\Delta m_{\perp}$ values (see illustrations in the Supplementary Material). To see separately the contribution from $\Delta m_{\perp}$ distortions we made additional calculations where we neglected the deviations for the $\Delta m_{\|}$-component and have set it to be exactly 1.0.

The calculated dipolar frequency patterns reveal astonishingly small deviations from the "classical" Pake shape up to the largest D-values tested. This results from a particular angular dependency of the distorting term in Eq. (8). The product $\sin(\theta)\cdot\cos(\theta)$ vanishes at both canonical orientations (θ=0 and θ=π/2). Because of this the positions of the "horns" and the left and right edges of the dipolar frequency pattern are very robust with respect to the amplitude of the distorting term (Figure 2). From the computed dipolar frequency patterns DEER traces for a fixed distance of 3 nm were constructed via proper scaling and Fourier transformation. Figure 5 shows a few examples of such calculations. The distance distributions obtained from these simulated DEER traces show very modest distortions which can be tolerated in many EPR based distance measurements.

The distance distortions due to the distributions of $\Delta m_{\|}$ values are very small for D≤600 MHz. Their contribution can be approximately accounted for by extra broadening of the obtained distance distributions according to the obtained widths for the distributions of $\Delta m_{\|}$. For D=300 MHz this extra broadening is already smaller than the artificial width of the distance distribution introduced by the Tikhonov regularization algorithm with the regularization parameter λ=0.001, which is the smallest value in the default regularization procedure of DeerAnalysis (see Supplementary Material). For D=600, 1500 and 2000 MHz a direct calculation of the dipolar frequency pattern distorted by the distributions of both $\Delta m_{\perp}$ and $\Delta m_{\|}$ values has been performed (Figure 5). These results are compared to the calculations with additional Gaussian distributions of the D-values with the width $\sigma=D/10$ and $\sigma=D/4$. If the distribution of D-values is sufficiently broad, the fraction of species with smaller D starts to determine the width of the distorted distance pattern, whereas species with larger D-values contribute to the extended wings of the distance pattern. The obtained distance distribution patterns resulting from a single distance define the best possible experimental distance resolution for each particular value of $3D/g\mu_B B$. Based on these simulations one can decide upon the applicability of a particular Gd^{3+}-complex for the planned distance measurements.

In the above analysis the excitation probabilities for all transitions were set to be equal in order to speed up the calculations. Including a correction for the transition moment will diminish the fraction of cases with strongest distortion, as these are also the cases where a reduced excitation probability is expected.

The presented analysis is valid for the Gd^{3+}-nitroxide DEER experiment. Analogous results are expected for DEER in other pairs with one half-integer high-spin centre and one spin 1/2 centre. In case of DEER between two high-spin species, like in Gd^{3+}-Gd^{3+} pairs, extra contributions have to be included in the dipolar term of the spin Hamiltonian. Most of the contributions will have a form of $I_{x,y}S_z$ or $I_zS_{x,y}$ and their influence will be

analogous to the distortion term analysed in detail above. An extra term, not existing in the distorted dipolar frequency pattern for Gd^{3+}-nitroxide pairs comes from spin products $I_{x,y}S_{x,y}$ and has an angular dependence proportional to $\sin^2(\theta)$. This term does not vanish at the orientations corresponding to the "horns" of the dipolar frequency pattern and thus would produce an important distortion. On the other hand, due to modulation depth reduction, Gd^{3+}-Gd^{3+} DEER is not a good experiment at X band and rather requires Q band or higher measurement frequencies. At these higher frequencies for most of Gd^{3+} centres the characteristic values of $\Delta m_\perp$ were computed to be below 1 and for the majority of orientations below 0.3. As the discussed extra term is also proportional to a square of the $\Delta m_\perp$, its influence on the measured distances should not be strong. In our case for a Gd^{3+} complex with D~1500 MHz the distribution of $\Delta m_\perp$ for the detection at Q band has to be somewhat narrower than the distribution of $\Delta m_\perp$ for D=600 MHz at X band. Therefore only very small distortions should be present in the obtained distance distribution. Taking into account that the experimentally obtained Gd^{3+}-Gd^{3+} distance distribution has a characteristic width of more than 1 nm, these distortions can be safely neglected. A detailed analysis of this term may be required if Gd^{3+}-Gd^{3+} distance measurements are performed at limiting conditions. The Q-band Gd^{3+}-Gd^{3+} distance measurements presented in this work as well as the Kα- and W-band Gd^{3+}-Gd^{3+} distance measurements reported so far[12-17] correspond to the cases of rather small ratios between ZFS and EZ terms in spin-Hamiltonian and do not require such a detailed analysis.

Analysis of obtained distance distributions: one sphere *vs.* two spheres description

For pairs of identical paramagnetic centres (two Gd^{3+} ions or two nitroxide radicals) a single sphere model is expected to be valid.[36,50] This model implies a point approximation for the paramagnetic centres and assumes that each centre is positioned randomly on a surface of a sphere with a particular radius. For a fixed sphere radius the probability to find a certain distance between two paramagnetic centres has a characteristic triangular shape with an average distance of 2/3 of the sphere diameter (Figure 6A). This model is, in general, not correct for an arrangement of two different types of paramagnetic ligands with different lengths of linkers as in the case of Gd^{3+}-nitroxide pairs. In that case in order to describe positions of the two types of paramagnetic centres one has to introduce two spheres of different size. The main differences between the two probability distributions, arising from the one-sphere and from the two-spheres model, are intuitively clear. First, as it is shown in Figure 6A, the two spheres distribution has a minimum distance cut-off. The minimal possible distance corresponds to the difference of the radii of the two spheres. The second feature of the two spheres distribution is that it has a more pronounced peak at the longest distance. If a distribution of sphere radii is present, these two features smear out as it is depicted in Figure 6B. Practically, assuming a radii distribution with a FWHM of 0.5-1.0 nm, one obtains nearly identical distributions for the single sphere model and for the two spheres model. The difference between the two distributions may grow when the difference of the two sphere radii increases. In the presented case one would need to detect minor differences in the shapes of the two distributions which requires experimental data of extremely good quality, not achievable due to measurement time restrictions. Because of this property we used the single sphere model already implemented in the DeerAnalysis to fit also Gd^{3+}-nitroxide distance measurements. For the two spheres case the single radius was interpreted as the arithmetic mean value of the radii of the two spheres. The model fits were in each case compared to the model-free fits of the experimental DEER traces.

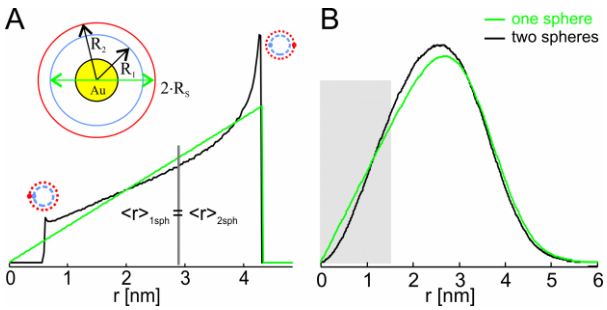

Figure 6 Comparison of distance distributions for one sphere and two spheres models. (A) Single sphere distance distribution (green) and two spheres distance distribution with R_2-R_1=0.5 nm (black). All sphere radii are fixed. Both distributions result in nearly the same mean distance, marked with the vertical black line. (B) Comparison of the two models for the case where all radii are distributed with Gaussian functions with the same mean values as in (A) and widths of 1 nm. The gray area indicates the range of distances not detectable in our DEER experiments.

Experimental results

The numerical analysis, given in the previous section shows, first of all, that in our DEER measurements with Gd^{3+}-DTPA complexes it is permissible to neglect ZFS-related distortions of dipolar frequencies. An additional simplification of the data analysis is the possibility to treat all three types of DEER data in terms of one sphere model without more detailed two spheres consideration. In case of Gd^{3+}-nitroxide distance measurements, the diameter of such an effective sphere has to be interpreted as the sum of two average distances from the centre of the AuNP to the two types of paramagnetic labels.

The observed modulation depths in nitroxide-nitroxide DEER measurements on different samples ranged between 0.12 and 0.23, which, for our experimental settings, implies a fraction of 1/4 to 1/2 of pairs among all detected nitroxide species. The modulation depths detected in Gd^{3+}-nitroxide DEER (~0.15-0.18 for 2% and 4% Gd^{3+}-loaded samples) also fit into this range. This is consistent with an assumption of statistically uniform and uncorrelated distributions of Gd^{3+} centres and nitroxide radicals over all AuNPs in each sample, and implies on average about 0.3 active nitroxide radicals per AuNP. Nevertheless this number should be considered as an estimate because of a polydispersity of NP sizes and compositions.

The overview of the experimental results and the distance distributions obtained with DeerAnalysis are shown in Figure 7. In contrast to the previous Gd^{3+}-nitroxide DEER measurements[21] we did not observe a significant decrease of the modulation depth at Q band compared to X band. Most probably, the reduction of the modulation depth in previous work was due to worse excitation profiles of the microwave pulses. In the present work a

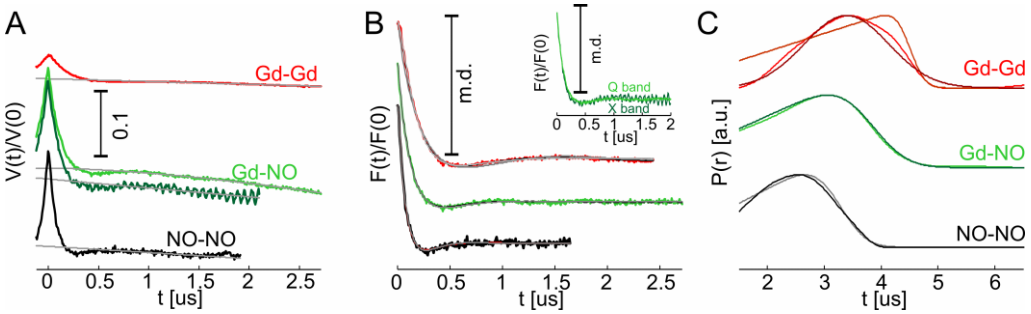

Figure 7 Experimental DEER traces for 4% Gd^{3+}-loaded AuNPs and their fits with DeerAnalysis software. (A) Experimental traces obtained in DEER experiment for Gd^{3+}-Gd^{3+} pairs at Q band (red), Gd^{3+}-nitroxide pairs at Q band (light green) and at X band (dark green), nitroxide-nitroxide pairs at Q band (black). The best background fits are shown in gray. (B) Intramolecular form factors for the three Q-band DEER traces from (A) with the same color code normalized by the modulation depth. Gray curves show the fits obtained with model free Tikhonov regularization (dark gray), sphere surface model fit (intermediate). For Gd^{3+}-Gd^{3+} DEER additionally a Gaussian fit of the distance distribution is shown in light gray color. (C) Distance distributions obtained for Gd^{3+}-Gd^{3+} (red), Gd^{3+}-nitroxide (green) and nitroxide-nitroxide (black). The model free fit is shown always in dark color, the sphere surface fit is shown in intermediate color and for Gd^{3+}-Gd^{3+} a Gaussian fit is shown in light red color.

new version of the same type of probehead[35] was used which may be responsible for the better performance of the DEER experiment. Still, since in our case the number of Gd^{3+}-nitroxide spin pairs is significantly less than the number of Gd^{3+} centres, the maximum expected modulation depth of 0.5 could not be reached and the possibility to obtain it at Q band still needs a direct verification.

Despite some variation in the modulation depth, the shape of obtained DEER traces is consistent for the nitroxide-nitroxide distance measurements in all four samples loaded with 0%, 2% and 4% of Gd^{3+} and with 32% of La^{3+}. Thus loading from zero to about 26 lanthanide ions per AuNP does not lead to measurable rearrangements of the nitroxide radical containing surface groups. The obtained nitroxide-nitroxide distance distributions are consistent with the single sphere model, which was discussed above, but two important remarks have to be done in this respect. First, the linker length for the nitroxide containing surface group is relatively short, therefore between 50% and 70% of the distance range falls into the suppression range of the DEER experiment and only about 30%-50% of the distribution, corresponding to the longer distance range, can be experimentally detected. Second, the sphere surface model is relatively unstable for the simultaneous increase of the width of the sphere size distribution and decrease of the average sphere size. The DEER pattern corresponding to the sphere surface model is characterized by an intense positive first 'half-oscillation', followed by a much shallower second negative half-oscillation. The presence and the shape of the second half-oscillation determine the width of the distribution of sphere sizes. At X band the obtained signal-to-noise levels were not sufficient to make an unambiguous interpretation of the second both for nitroxide-nitroxide and for Gd^{3+}-nitroxide distance measurements. At Q band the analysis was directly possible for Gd^{3+}-nitroxide DEER traces. For nitroxide-nitroxide distance measurements, due to lower overall S/N ratios, it required careful verification of the background behaviour for longer time traces with following measurement of the DEER trace with the length just sufficient for the separation between the background and the form factor.

For the Gd^{3+}-nitroxide DEER experiment, the best agreement of the form factor fit to the experimental data was achieved for the background dimension of 4.6-4.8. The increase of the apparent background dimension is sometimes observed in DEER experiment and may be due to the presence of excluded volumes in the vicinity of the detected spins.[51] In our case such excluded volumes could be due to the presence of the Au-nanoparticles. Each detected spin would have a nanoparticle close to it and this would lead to the distortion of homogeneous 3D distribution of surrounding spins.

The Gd^{3+}-nitroxide DEER traces of each sample obtained at X band and at Q band were identical within the experimental precision which includes the noise level and the level of incompletely averaged proton ESEEM oscillations observed in the X-band measurements (see inset in Figure7B). For the two samples with 2% and 4% Gd^{3+} loading the differences in the shapes of the Gd^{3+}-nitroxide DEER traces were minor and did not lead to significant differences in the obtained distance distributions.

At Q band the Gd^{3+}-nitroxide DEER experiment resulted in very similar distance distributions for 2% and 4% Gd^{3+}-loaded samples. The distance distributions could be well fitted with a single sphere model with an average sphere size of 3.6 nm and 3.7 nm, and with the half-width of sphere size distribution ($\sigma(r)$) of 0.7 nm. In nitroxide-nitroxide DEER the corresponding values for the sphere size were 3.13 nm and 3.2 nm,with $\sigma(r)$=0.7 nm and 0.5 nm. For both samples model free fits and sphere surface fits were resulting in very similar time traces and provided nearly identical agreement to the experimental data independent on the choice of the background model (Figure 7C).

In the Gd^{3+}-Gd^{3+} DEER measurement yet longer distances were detected and therefore the fraction of the time trace available for the background fit was rather short. For most choices of the interval for the background fit the optimum background dimension was 3.0-3.15. In some cases the background model attempted to incorporate the second half-oscillation into the background, which resulted in background dimension of about 8. Even for those cases, the obtained distance distribution did not change strongly and the cut-off distance as well as the width of the obtained distribution remained approximately the same. In all cases the fraction of species with Gd^{3+}-Gd^{3+} distances below 2.5 nm was clearly less than the amount predicted by the single sphere model. The Gd^{3+}-Gd^{3+} distance distribution could be well fitted with a Gaussian model

(and with the model free fit). The fitted mean distance and the half-width of the distribution were 3.4 nm and 1.0 nm, respectively.

The effective sphere size increased by about 0.5 nm for Gd^{3+}-nitroxide spin pairs as compared to the nitroxide-nitroxide case for both 2% and 4% Gd^{3+}-loaded samples. The estimate of the lengths of two types of linkers (S-Gd^{3+} distance ~1.4 nm, S-N distance ~0.95 nm) gives difference of about 0.4 nm in the longest conformation. The remaining mismatch can be attributed to the precision of the distance measurements and to possible conformational details of both functional groups on the surface of AuNP. As the single sphere model did not fit well to the Gd^{3+}-Gd^{3+} DEER data, a direct comparison of the effective sphere size was not possible for that case. Still, from Figure 7C one can see that the falling slopes of all three distance distributions have similar shapes and their positions follow approximately the same step of about 0.5 nm. Assuming an average size of AuNP to be 2.42 nm and the width of particle size distribution to be 0.34 nm (see supplementary information for TEM data) one would expect the cut-off distance to be about 5.5 nm for Gd^{3+}-Gd^{3+} distance measurements. This estimate assumes the largest size of AuNP and the longest conformation of both Gd^{3+}-DTPA linkers. The experimental distance distribution obtained with model free fit shows cut-off at around 5.0-5.1 nm. The observed discrepancy of about 0.4 nm can be attributed to i) precision of the particle diameter determination with TEM and ii) distribution of linker conformations, in which the longest conformation is not the most populated one. In analogy to these estimates the cut-off distances for the Gd^{3+}-nitroxide distance distribution should be about 5.0-5.1 nm and for the nitroxide-nitroxide distance measurement the cut-off distance should be around 4.6 nm. Again the observed cut-off distances are about 0.4-0.5 nm shorter as compared to these estimates. On the other hand the change of the cut-off distance in the series nitroxide-nitroxide, Gd^{3+}-nitroxide, Gd^{3+}-Gd^{3+} fits rather well to the difference in linker length.

In the Gd^{3+}-nitroxide DEER experiment a reduction of the amplitude of the refocused echo down to approximately 30% of its original value was observed upon applying the pump pulse. The magnitude of the effect did not change to a detectable extent by changing the second interpulse delay of the refocused echo pulse sequence. At X band it also did not change significantly upon setting the pump pulse on the opposite (high field) side of the Gd^{3+} central peak, such that no (or strongly reduced) overlap of the pump pulse excitation profile with the nitroxide spectrum was ensured. At Q band such a mirrored setup of the pump pulse lead to yet stronger reduction of the DEER echo. Some further details are given in the Supplementary Material. The echo reduction with the mirrored setup indicates that this is an intrinsic property of Gd^{3+} centres and that it is related to their response on the pump pulse rather than to the interaction of Gd^{3+} centres with nitroxide radicals. The independence of the effect on the second interpulse delay implies that the processes responsible for the echo reduction take place during the pump pulse and do not lead to further phase drift or echo amplitude reduction during the following time evolution of the magnetisation. Thus the influence of the echo reduction effect must be restricted to the reduction of the obtained signal-to-noise ratio, but it should not have influenced the obtained distance distributions.

The signal-to-noise values calculated for 2% Gd^{3+} loaded sample per single shot were about a factor of 3-4 better for the Gd^{3+}-nitroxide DEER experiment as compared to the nitroxide-nitroxide DEER experiment (see Supplementary Materials). Approximately the same sensitivity ratios between Gd^{3+}-nitroxide DEER and nitroxide-nitroxide DEER were obtained for X-band and for Q-band measurements, indicating that the extra increase of the sensitivity due to the narrowing of the central transition of Gd^{3+} species at Q band is not very strong for this type of chelate complexes. For the 2% Gd^{3+} loaded sample, a 4-8-fold excess of Gd^{3+} centres to the number of nitroxide radicals per AuNP was estimated. Thus, in this case the sensitivity of the two types of distance measurements differs by approximately a factor of 1.5-3.0 for X and Q band if computed per shot and per unit spin concentration. For the Gd^{3+} centres 1.6 times faster repetition was possible, which further increased the sensitivity of Gd^{3+}-nitroxide DEER experiment if computed per unit time. The overall sensitivity of Gd^{3+}-nitroxide DEER can therefore be estimated to be somewhat lower but rather close to the sensitivity of nitroxide-nitroxide DEER. The characteristic transverse relaxation time T_2 of the nitroxide radicals measured at DEER detection temperature (50 K) was comparable to the corresponding average T_2 of the Gd^{3+} ions, measured at 10 K (see Supplementary Material). In addition the signal-to-noise ratios for Gd^{3+}-nitroxide and Gd^{3+}-Gd^{3+} DEER were computed on the 4% Gd^{3+} loaded sample (see Supplementary Material). The two experiments show comparable sensitivity with possibly some advantage for the Gd^{3+}-nitroxide DEER.

Discussion

We could prove numerically and experimentally on AuNPs that DTPA-based tags for chelating Gd^{3+} ions allow for reliable distance measurements both between the Gd^{3+} ion and a nitroxide label at X- and Q-band frequencies and between two Gd^{3+} ions at Q-band frequencies. The Gd^{3+}-nitroxide DEER traces measured at X and Q band nicely superimpose. From that we can conclude that even in the sensitive range around the cut-off distance distortions of the distance distribution are rather minor. The obtained distance distributions for nitroxide-nitroxide, Gd^{3+}-nitroxide and Gd^{3+}-Gd^{3+} pairs reveal a characteristic increase of the cut-off distance that is consistent with the difference in the lengths of the two spin-label-functionalized ligands. Potentially such measurements in conjunction with TEM can help to establish the conformation of different tethered ligands on the nanoparticle surface. Additionally, the EPR data can provide information on the homogeneity of distribution of ligands on the nanoparticle surface. For nanoparticles with a mixed ligand shell, this is quite important as it makes it possible to distinguish between a homogeneous distribution, as we find it here, and microphase separation. For many applications, which rely on molecular recognition (e.g., biological/medicinal), this nature of the distribution of ligands in the mixed shell is quite important. Similar issues can turn up in the characterization of micelles, which has been previously studied by DEER techniques.[52,53]

The numerical analysis we presented in this paper deals with secular contributions to the dipolar frequencies. The effect of non-secular terms was discussed in some detail previously.[13] It was pointed out that the magnitude of pseudo-secular terms is

bigger for a pair of high spins as compared to the pair of nitroxide radicals with spins 1/2. It was suggested that because of this, the resonance offset of about 150-200 MHz used in the Gd^{3+}-Gd^{3+} DEER experiments may not be sufficiently large to neglect the contributions from the pseudosecular terms. The main consequences of having these terms in the dipolar interaction were proposed to be a reduction of the DEER modulation depth and a shift of the apparent dipolar frequency.

From our set of experimental data we cannot analyze this effect in detail for the presented Gd^{3+}-Gd^{3+} DEER measurements. Still the detected increase of the cut-off distance is in line with the three obtained distance distributions (nitroxide-nitroxide, Gd^{3+}-nitroxide and Gd^{3+}-Gd^{3+}) and follows the expectations from the length difference of the two linkers. Thus we can assume that distortions of obtained distances in the cut-off range are not large in the Gd^{3+}-Gd^{3+} DEER experiment. For shorter distances the discussed effect may play a more significant role, thus the above mentioned depletion of shorter distances in the Gd^{3+}-Gd^{3+} distance distribution may not be as strong as it appears from the distance analysis with a standard algorithm used in the DeerAnalysis software.

For the Gd^{3+}-nitroxide DEER a more detailed analysis of the contributions from the pseudosecular terms can be done, because the data detected at two different frequencies (X and Q band) are available. In a Gd^{3+}-nitroxide spin pair only one of the two spins (Gd^{3+}) has increased values of the spin-operator matrix elements, therefore the magnitude of the pseudosecular term is reduced in this case compared to the pair of Gd^{3+} ions. By changing the detection frequency from X band to Q band, which at the same time implies a change of the frequency offset from about 85 to 300 MHz, neither a change of the modulation depth nor a significant change of the shape of the DEER trace and the obtained distance distribution has been observed (Figure 7B, inset). On the basis of these results we assume that in this experiment the role of pseudosecular terms is restricted to producing distortions for a small fraction of spin pairs for which the two frequencies are in the range where the pump and detection pulse excitation profiles overlap. Apparently, this problematic range is not much bigger than in the case of the nitroxide-nitroxide DEER experiment and it still allows for a correct detection of distances.

A clear advantage of the use of orthogonal spin labels is the possibility to perform three independent distance measurements on the same sample. The selective detection of the three distance distributions is based on the following main principles.[21] First, there is a significant difference of the optimum pulse settings for the two types of spin centres owing to the different transition moments for single-quantum transitions. Second, for pumping or detecting on Gd^{3+} ions, the corresponding frequencies can be set outside of the nitroxide spectral range (Figure 1). And third, the difference in the longitudinal relaxation times of Gd^{3+} and nitroxide helps in Gd^{3+}-nitroxide DEER at X-band where slight overlap of the detection pulse bandwidth with the spectrum of the pumped nitroxide spins is present. In the presented case the longitudinal relaxation of Gd^{3+} is slower than for the previously reported complex of $Gd^{3+}$with terpyridine derivative.[21] Still T_1 time of Gd^{3+} is well below 1 ms at 10 K and thus the difference in relaxation times of Gd^{3+} centres and nitroxide radicals (T_1~10^2 ms at T=10 K) is about two orders in magnitude.

The echo reduction effect in the Gd^{3+}-nitroxide DEER experiment needs to be analysed in detail. This work is currently in progress and will be a matter of a separate publication. At present we can argue that at least partially this effect might be related to the transfer of the single quantum coherence on $|-1/2\rangle\leftrightarrow|+1/2\rangle$ transition to double-quantum coherences on $|-1/2\rangle\leftrightarrow|+3/2\rangle$ and on $|-3/2\rangle\leftrightarrow|+1/2\rangle$ transitions and possibly to further high order coherences upon applying the pump pulse. A simple illustration of such a process is given in the Supplementary Materials. The understanding of the echo reduction mechanism and corresponding optimization of the measurement conditions could allow for a significant sensitivity improvement in the Gd^{3+}-nitroxide DEER experiment.

Concerning the presented dipolar frequency analysis, some important predictions about the achievable resolution can be made. The width of the distance distribution, originating from the distorted dipolar frequency pattern in the Gd^{3+}-nitroxide DEER experiment, depends on the characteristic value of D for the type of Gd^{3+} complexes used in this work. Depending on what kind of distance information is required, the limiting value of D that still allows for obtaining this information has to be set differently. The most sensitive type of problem would be an analysis of the shape of a narrow distance distribution or resolving two overlapping peaks with small difference of the mean distances. In this case the resolution is limited by the width of the DEER-distance pattern originating from a single distance due to the distortions. If systems with well defined distances between two paramagnetic centres are studied,[54-59] a distance resolution of 0.3 Å or even better may be required. For such cases, if distance measurements are performed at X band Gd^{3+} complexes with $D\leq600$ MHz should provide sufficiently narrow distance patterns for distances around 3 nm or below. The width of the distorted distance pattern scales with the distance and the resolution of 0.3 Å at 3 nm distance would reduce to a resolution of only 1 Å if a distance of about 10 nm has to be measured. Because of this, for distances of about 8-10 nm higher relative precision is needed to provide the same absolute distance resolution. In this case the value of D needs to be further restricted to be below ~300 MHz. For less critical cases[60] complexes with larger D-values can be utilized. In any case for limiting values of D a careful estimate of the actual width of the distorted single distance pattern is required and deconvolution analysis may be necessary for obtaining some particular details.

If the cut-off distances for two particular distance distributions have to be compared the best achievable resolution should normally be better than the width of the distorted single distance pattern. In this case the proof of the stability of such distorted single distance patterns is required, which can be obtained by measuring ED or CW EPR spectra of the two samples and confirming that the shapes of Gd^{3+} absorption lines are the same.

The most robust parameter is the mean distance, which at X band seems to be nearly undisturbed for D up to 1000 MHz for a 3 nm distance. For distances around 10 nm and a value of D~1500 MHz a precision of 1 Å is expected for mean distance measurements.

At higher measurement frequencies the limiting D-values scale up according to the frequency increase. Therefore, at Q band (35

GHz) the limiting *D*-value for the sensitive narrow distance distribution shape analysis should scale up to about 1000 MHz for the longest distances (~10 nm). For distances around 3 nm the limiting *D*-value would be about 2000 MHz, which covers a number of the commonly used chelate complexes of Gd^{3+}.[19,20,49,61] At W band all types of distance measurements with Gd^{3+}-nitroxide DEER should be possible with sufficient resolution for the complexes with $D \leq 3000$ MHz.

For distance measurements in spin-labelled biomolecules a resolution of 1-2 Å is sufficient in almost all cases, even if rigid spin labels are in use. Narrow distance distributions are most frequently obtained in measurements on spin-labelled nucleic acids[62-64] but can also appear in the protein studies.[65-69] Still, especially in DEER measurements on proteins there are many cases when the widths of the obtained distance distributions are of about 1 nm or even broader.[70-79] At X-band, for those situations even the use of Gd^{3+} complexes with *D*~1500 MHz for distances up to 10 nm or *D*~2000 MHz for distances up to 3 nm can be permissible, perhaps with an additional deconvolution analysis of the obtained distance distributions. Complexes with *D*~1000 MHz should allow for X-band distance measurements without a need of deconvolution for almost all cases except the very narrow 0.2-0.4 nm wide distributions at long distances. At Q band all types of distance measurements on biomolecules with Gd^{3+}-nitroxide DEER should be possible without deconvolution analysis for Gd^{3+}-complexes with $D \leq 2000$ MHz.

Conclusions

We have demonstrated that the use of Gd^{3+} ions in combination with nitroxide radicals allows for selective detection of three types of distance distributions in the same sample. The presented dipolar frequency analysis shows that distance measurements with use of Gd^{3+} ions as spin labels are at most only moderately disturbed by the interplay between ZFS and EZ interactions. In the case of Gd^{3+}-nitroxide DEER, distance measurements can be performed on the majority of commonly used Gd^{3+} chelate complexes down to X-band frequencies.

Note at revision

The concept of selective distance measurements in nitroxide- and Gd^{3+}-containing systems has been previously introduced at a conference and in a thesis.[80] After initial submission of this work we became aware of a Communication[81] that demonstrates this concept on a model protein labeled with a racemic mixture of nitroxide- and Gd^{3+}-tags and suggests an alternative explanation for the echo reduction effect.

Acknowledgements

Authors thank Dr. Yevhen Polyhach and Dr. Enrica Bordignon for numerous fruitful discussions of the work and Rene Tschaggelar for technical support. The work was funded by the SNF grant 200021_121579. VC and MW would like to thank Higher Education Commission (HEC) of Pakistan and The University of York (Wild Fund) for financial support.

Notes and references

a Laboratory of Physical Chemistry, ETH Zurich, Wolfgang Pauli Str.10, 8093, Zurich, Switzerland. Fax: +41 44 633 1448; Tel: +41 44 632 3118; E-mail: maxim.yulikov@phys.chem.ethz.ch

b Department of Chemistry, University of York, Heslington, York YO10 5DD, UK. Fax: +44 1904 322516; Tel: +44 1904 324185; E-mail: victor.chechik@york.ac.uk

c Present address: Chemistry Department, Baghdad-ul-Jaded Campus, The Islamia University of Bahawalpur, Bahawalpur-63100, Pakistan

† Electronic Supplementary Information (ESI) available: [Characterization of Au-nanoparticles; Fitting of the ZFS parameter *D* from Gd^{3+} ED EPR spectra; Numeric calculations of dipolar frequencies for different ZFS parameters; Evaluation of the signal-to-noise ratios in nitroxide-nitroxide, Gd^{3+}-nitroxide and Gd^{3+}- Gd^{3+} DEER measurements; T_1 and T_2 times of Gd^{3+} ions and nitroxide radicals; Echo reduction effect and its tentative interpretation; DEER measurements at X and Q band]. See DOI: 10.1039/b000000x/

1 D.L. Farrens, C. Altenbach, K. Yang, W.L. Hubbell, H. Gobind Khorana, *Science*, 1996, **274**, 768 – 770; W.L. Hubbell, D.S. Cafiso and C. Altenbach, *Nature*, 2000, **7**, 735 – 739.

2. A.D. Milov, K.M. Salikhov and M.D. Shirov, *Fiz. Tverd. Tela (Leningrad)* 1981, **23**, 957 – 982; A.D. Milov, A.B. Ponomarev and Yu.D. Tsvetkov, *Chem. Phys. Lett.* 1984**,** **110**, 67 – 72.

3. M. Pannier, S. Veit, A. Godt, G. Jeschke and H.W. Spiess, *J. Magn. Reson.,* 2000, **142**, 331 – 340.

4. G. Jeschke and Ye. Polyhach, *Phys. Chem. Chem. Phys.,* 2007, **9**, 1895 – 1910; O. Schiemann and T.F. Prisner, *Q. Rev. Biophys.,* 2007, **40**, 1 – 53; E. Bordignon, *Curr. Top. Chem*., 2011, Sep 7. [Epub ahead of print].

5. C. Elsaesser, M. Brecht and R. Bittl., *J. Am. Chem. Soc*. 2002, **124**, 12606 – 12611; C. Elsaesser, M. Brecht and R. Bittl., *Biochem. Soc. Trans*. 2005, **33**, 15 – 19.

6. I.M. van Amsterdam, M. Ubbink, G.W. Canters and M. Huber, *Angew. Chem. Int. Ed*., 2003, **42**, 62 – 64.

7. C.W. Kay, H.E. Mkami, R. Cammack and R.W. Evans, *J. Am. Chem. Soc*., 2007, **129**, 4868 – 4869.

8. E. Narr, A. Godt and G. Jeschke, *Angew. Chem. Int. Ed*., 2002, **41**, 3907 – 3910.

9. B.E. Bode, J. Plackmeyer, T.F. Prisner and O. Schiemann, *J. Phys. Chem. A*, 2008, **112**, 5064 – 5073.

10. J.E. Lovett, A.M. Bowen, C.R. Timmel, M.W. Jones, J. R. Dilworth, D. Caprotti, S.G. Bell, L.L. Wong and J. Harmer, *Phys. Chem. Chem. Phys*., 2009, **11**, 6840 – 6848.

11. Z. Yang, D. Kise and S. Saxena, *J. Phys. Chem. B*, 2010, **114**, 6165 – 6174.

12. A.M. Raitsimring, C. Gunanathan, A. Potapov, I. Efremenko, J.M.L. Martin, D. Milstein and D. Goldfarb, *J. Am. Chem. Soc*., 2007, **129**, 14138 – 14139.

13. A. Potapov, Y. Song, T.J. Meade, D. Goldfarb, A.V. Astashkin and A.M. Raitsimring, *J. Magn. Reson*., 2010, **205**, 38 – 49.

14. A. Potapov, H. Yagi, T. Huber, S. Jergic, N.E. Dixon, G. Otting and D. Goldfarb, *J. Am. Chem. Soc*., 2010, **132**, 9040 – 9048.

15. M. Gordon-Grossman, I. Kaminker, Y. Gofman, Y. Shai and D. Goldfarb, *Phys. Chem. Chem. Phys*., 2011, **13**, 10771 – 10780.

16. H. Yagi, D. Banerjee, B. Graham, T. Huber, D. Goldfarb and G. Otting, *J. Am. Chem. Soc*., 2011, **133**, 10418 – 10421.

17. Y. Song, T.J. Meade, A.V. Astashkin, E.L. Klein, J.H. Enemark and A. Raitsimring, *J. Magn. Reson*., 2011, **210**, 59 – 68.

18. X.-C. Su and G. Otting, *J. Biomol. NMR*, 2010, *46*, 101 – 112; P.H.J. Keizers and M. Ubbink, *Progr. in NMR Spectr*., 2011, **58**, 88 – 96.

19. A.M. Raitsimring, A.V. Astashkin, O.G. Poluektov and P. Caravan, *Appl. Magn. Reson*. 2005, **28**, 281 – 295;

20. A.M. Raitsimring, A.V. Astashkin and P. Caravan, *Biological Magnetic Resonance*, ed. G. Hanson and L.J. Berliner, Springer, New York, 2009, **28**, 581 – 621.

21. P. Lueders, G. Jeschke and M. Yulikov, *J. Phys. Chem. Lett*. 2011, **2**, 604 – 609.

22. S. Cotton, *Lanthanide and Actinide Chemistry*, John Wiley and Sons, 2006.

23. A.G. Maryasov, M.K. Bowman and Yu.D. Tsvetkov, *Appl. Magn. Reson*., 2006, **30**, 683 – 702.

24. G. Jeschke, H. Zimmermann and A. Godt, *J. Magn. Reson*., 2006, 180, 137 – 146.
25. M.-C. Daniel and D. Astruc, *Chem. Rev.,* 2004, **104,** 293.
26. P. Ionita, A. Caragheorgheopol, B. C. Gilbert and V. Chechik, *J. Phys. Chem. B,* 2005, **109,** 3734.
27. P. Ionita, A. Volkov, G. Jeschke and V. Chechik, *Anal. Chem.,* 2008, **80**, 95.
28. M. F. Warsi, R. W. Adams, S. B. Duckett and V. Chechik, *Chem. Comm.,* 2010, **46,** 451.
29. V. Chechik, H. J. Wellsted, A. Korte, B. C. Gilbert, H. Caldararu, P. Ionita and A. Caragheorgheopol, *Faraday Discuss.,* 2004, **125,** 279.
30. M. Brust, M. Walker, D. Bethell, D. J. Schiffrin and R. Whyman, *J. Chem. Soc., Chem. Commun.*, 1994, 801.
31. P. Ionita, A. Caragheorgheopol, B. C. Gilbert and V. Chechik, *Langmuir,* 2004, **20,** 11536.
32. S. Langereis, Q. G. de Lussanet, M. H. P. van Genderen, W. H. Backes and E. W. Meijer, *Macromolecules*, 2004, **37**, 3084.
33. P.-J. Debouttière, S. Roux, F. Vocanson, C. Billotey, O. Beuf, A. Favre-Réguillon, Y. Lin, S. Pellet-Rostaing, R. Lamartine, P. Perriat and O. Tillement, *Adv. Funct. Mater.,* 2006, **16,** 2330.
34. I. Gromov, J. Shane, J. Forrer, R. Rakhmatoullin, Y. Rozentzwaig, and A. Schweiger, *J. Magn. Reson*., 2001, **149**, 196–203.
35. R. Tschaggelar, B. Kasumaj, M.G. Santangelo, J. Forrer, P. Leger, H. Dube, F. Diederich, J. Harmer, R. Schuhmann, I. García-Rubio, *et al*., *J. Magn. Reson*., 2009, **200**, 81 – 87.
36. G. Jeschke, V. Chechik, P. Ionita, A. Godt, H. Zimmermann, J. Banham, C.R. Timmel, D. Hilger and H. Jung, *Appl. Magn. Reson.*, 2006, **30**, 473 – 498; http://www.epr.ethz.ch/software/index.
37. A.N. Tikhonov, V.Y. Arsenin, in: *Solutions of Ill-Posed Problems*, New York: Wiley 1977.
38. G. Jeschke, G. Panek, A. Godt, A. Bender, and H. Paulsen, *Appl. Magn. Reson*., 2004, **26**, 223-244.
39. Y.W. Chiang, P.P. Borbat, J.H. Freed, *J. Magn. Reson*., 2005, **172**, 279–295.
40. S. Stoll and A. Schweiger, *J. Magn. Reson*., 2006, **178**, 42 – 55.
41. A.M. Raitsimring, A.V. Astashkin, *J. Chem. Phys*. 2002, **117**, 6121 – 6132.
42. H.A. Buckmaster, Y.H. Shing, *Phys. Stat. Sol*. (A), 1972, **12**, 325-361.
43. C.P. Slichter, *Principles of magnetic resonance*, Springer Series in Solid-State Sciences 1, Springer-Verlag Berlin Heidelberg, 1978.
44. A. Abragam, *Principles of nuclear magnetism*, International Series of Monographs on Physics – 32, Oxford University Press, New York, 1982.
45. A. Schweiger and G. Jeschke, *Principles of pulse electron paramagnetic resonance*, Oxford University Press, Oxford, 2001.
46. G.E. Pake, *J. Chem. Phys*., 1948, **16**, 327-336.
47. A. Abragam, B. Bleaney, *Electron Paramagnetic Resonance of Transition Metal Ions*, Clarendon Press, 1970.
48. B. Bleaney, R.S. Rubins, *Proc. Phys. Soc*., 1961, **77**, 103 – 112.
49. M. Benmelouka, J. Van Tol, A. Borel, S. Nellutla, M. Port, L. Helm, L.-C. Brunel and A.E. Merbach, *Helvetica Chimica Acta*, 2009, **92**, 2173 – 2185.
50. P. Ionita, A. Volkov, G. Jeschke and V. Chechik, *Anal. Chem*. 2008, **80**, 95 – 106.
51. M.J.N. Junk, H.W. Spiess and D. Hinderberger, *J. Magn. Reson*., 2011, **210**, 210 – 217.
52. S. Ruthstein, A.M. Raitsimring, R. Bitton, Veronica Frydman, A. Godt and D. Goldfarb, *Phys. Chem. Chem. Phys*., 2009, **11**, 148–160
53. S. Ruthstein, A. Potapov, A.M. Raitsimring, and D. Goldfarb, *J. Phys. Chem. B* 2005, **109**, 22843-22851
54. A. Godt, M. Schulte, H. Zimmermann and G. Jeschke, *Angew. Chem. Int. Ed*., 2006, **45**, 7560 – 7564.
55. Ye. Polyhach, A. Godt, C. Bauer and G. Jeschke, *J. Magn. Reson*., 2007, **185**, 118 – 129.
56. D. Margraf, B.E. Bode, A. Marko, O. Schiemann and T.F. Prisner, *Molecular Physics*, 2007, **105**, 2153-2160.
57. J.E. Lovett, M. Hoffmann, A. Cnossen, A.T.J. Shutter, H.J. Hogben, J.E. Warren, S.I. Pascu, C.W.M. Kay, C.R. Timmel and H.L. Anderson, *J. Am. Chem. Soc*., 2009, **131**, 13852 – 13859.
58. M. Sajid, G. Jeschke, M. Wiebcke and A. Godt, *Chem. Eur. J*. 2009, **15**, 12960 – 12962.
59. G. Jeschke, M. Sajid, M. Schulte, N. Ramezanian, A. Volkov, H. Zimmermann and A. Godt, *J. Am. Chem. Soc*., 2010, **132**, 10107 – 10117.
60. D. Kurzbach, D.R. Kattnig, B. Zhang, A. Dieter Schlüter and D. Hinderberger, *J. Phys. Chem. Lett*., 2011, **2**, 1583 – 1587.
61. M. Benmelouka, J. Van Tol, A. Borel, M. Port, L. Helm, L.-C. Brunel and A.E. Merbach, *J. Am. Chem. Soc*., 2006, **128**, 7807 – 7816.
62. I. Krstic, R. Hänsel, O. Romainczyk, J.W. Engels, V. Dötsch and T.F. Prisner, *Angew. Chem. Int. Ed*., 2011, 50, 5070 – 5074.
63. O. Romainczyk, B. Endeward, T.F. Prisner and J.W. Engels, *Mol. BioSyst*., 2011, **7**, 1050 – 1052.
64. A. Marko, V. Denysenkov, D. Margraf, P. Cekan, O. Schiemann, S.Th. Sigurdsson and T.F. Prisner, *J. Am. Chem. Soc*. 2011, **133**, 13375 – 13379.
65. Z. Zhou, S.C. DeSensi, R.A. Stein, S. Brandon, M. Dixit, E.J. McArdle, E.M. Warren, H.K. Kroh, L. Song, C.E. Cobb, E.J. Hustedt and A.H. Beth, Biochemistry, 2005, **44**, 15115 – 15128.
66. C. Dockter, A. Volkov, C. Bauer, Ye. Polyhach, Z. Joly-Lopez, G. Jeschke and H. Paulsen, *Proc. Acad. Sci. USA*, 2009, **106**, 18485 – 18490.
67. B. Endeward, J.A. Butterwick, R. MacKinnon and T.F. Prisner, *J. Am. Chem. Soc*., 2009, **131**, 15246 – 15250.
68. G. Jeschke, A. Bender, T. Schweikardt, G. Panek, H. Decker and H. Paulsen, *J. Biol. Chem*., 2005, **280**, 18623 – 18630.
69. B. Vileno, J. Chamoun, H. Liang, P. Brewer, B.D. Haldeman, K.C. Facemyer, B. Salzameda, L. Song, H.-C. Li, C.R. Cremo and P.G. Fajer, *Proc. Acad. Sci. USA*, 2011, **108**, 8218–8223.
70. D. Hilger, Ye. Polyhach, H. Jung and G. Jeschke, *Biophys. J*., 2009, **96**, 217 – 225.
71. E.R. Georgieva, T.F. Ramlall, P.P. Borbat, J.H. Freed and D. Eliezer, *J. Biol. Chem*., 2010, **285**, 28261 – 28274.
72. J. Bhatnagar, P.P. Borbat, A.M. Pollard, A.M. Bilwes, J.H. Freed and B.R. Crane, *Biochemistry*, 2010, **49**, 3824 – 3841.
73. R. Ward, A. Bowman, E. Sozudogru, H. El-Mkami, T. Owen-Hughes and D.G. Norman, *J. Magn. Reson*., 2010, **207**, 164 – 167.
74. S. Böhme, H.-J. Steinhoff and J.P. Klare, *Spectroscopy*, 2010, **24**, 283 – 288.
75. I. Krstić, O. Frolow, D. Sezer, B. Endeward, J.E. Weigand, B. Suess, J.W. Engels and T.F. Prisner, *J. Am. Chem. Soc*., 2010, **132**, 1454 – 1455.
76. G. Phan, H. Remaut, T. Wang, W.J. Allen, K.F. Pirker, A. Lebedev, N.S. Henderson, S. Geibel, E. Volkan, J. Yan *et. al*., *Nature*, 2011, **474**, 49 – 53.
77. N. Van Eps, A.M. Preininger, N. Alexander, A.I. Kaya, S. Meier, J. Meiler, H.E. Hamm and W.L. Hubbell, *Proc. Acad. Sci. USA*, 2011, **108**, 9420 – 9424.
78. B.E. Bode, R. Dastvan, T.F. Prisner, *J. Magn. Reson*., 2011, **211**, 11 – 17.
79. M. Herget, C. Baldauf, C. Schölz, D. Parcej, K.-H. Wiesmüller, R. Tampé, R. Abele and E. Bordignon, *Proc. Acad. Sci. USA*, 2011, **108**, 1349 – 1354.
80. P. Lueders, M.Yulikov and G.Jeschke, JEOL prize talk (T10) and poster(P10), The 44th annual international meeting of the ESR spectroscopy group of the RSC, York 3rd-7th April 2011; P. Lueders PhD thesis, ETH Zurich 2011.
81. I. Kaminker, H. Yagi, T. Huber, A. Feintuch, G. Otting and D. Goldfarb, *Phys. Chem. Chem. Phys*., 2012, **14**, 4355–4358.